URSI-RCRS 2024, ARIES/GEHU, Bhimtal, India, 22 - 25 October, 2024

Deep-Learning Assisted Tomographic Reconstruction of Buried Objects

Mallikarjun Erramshetty(1), Harisha S B(2)
(1)Department of Electronics and Communication Engineering, National Institute of Technology Goa, Goa, India, emallikarjuna@nitgoa.ac.in
(2)Department of Electronics and Communication Engineering, National Institute of Technology Goa, Goa, India, harishasb@jnnce.ac.in

Abstract

This paper explores the use of deep learning (DL) for tomographic reconstruction of dielectric objects with ground penetrating radar, employing a bistatic multi-frequency imaging setup. A U-Net based convolutional neural network is trained using outputs from inverse algorithms to enhance the quality of reconstructed images. Numerical experiments demonstrate significant improvements in detection accuracy, thereby advancing the capabilities of tomographic imaging in complex environments.

Index Terms - Deep learning, dielectrics, detection, tomographic detection, image configuration.

1. Introduction

Ground-Penetrating Radar (GPR) is widely used in military, civil, and archaeological applications [1]. Traditional GPR methods generate 2-D radargrams to infer object locations, but they lack details on electrical properties and geometric features, complicating their use in complex scenarios. Tomographic GPR overcomes some of these limitations by solving scattered field integral equations. However, these problems are highly non-linear, making them unsuitable for real-time applications. To address this, the Born Approximation (BA) is adopted for a linear inverse solution, enhancing practicality [2].

The tomographic approach faces challenges such as accuracy, resolution, and noise impact. This research addresses these challenges using deep learning (DL) [3]. A new DL based methodology employs inverse algorithms to roughly estimate buried objects, which are then used to train a U-Net based convolutional neural network [4]. This network maps the inverse algorithm outputs to the corresponding ground truth profiles.

Once trained, the network serves as a post-processing tool to enhance the quality of images reconstructed through inverse algorithms. Various numerical examples are considered to validate the approach, and the results are compared to demonstrate improvements in image quality and detection accuracy. By integrating DL with GPR, the research aims to overcome existing limitations and advance the field of tomographic imaging.

2. Problem Formulation

For simplicity, two-dimensional (2D) scalar scenario is considered and it is made of two homogeneous half spaces separated by a plane of $y = 0$. The upper half is free space, whereas the lower one has complex permittivity of ϵ_b and the target objects are buried within. The object dimensions along z-axis is infinite. If the target objects are illuminated by a transmitting antenna (Tx) from upper half space, and the incident field is polarized along z-axis, then, Born's approximated scattering equations for this problem, can be written synthetically as [5]

$$\boldsymbol{G}[\chi] = \boldsymbol{f} \qquad (1)$$

where $\boldsymbol{f}$ indicates scattered electric fields, respectively, $\boldsymbol{G}$ is a mapping function from object's domain to scattered field domain, and χ is the object's contrast function that can be expressed as $\chi = \left(\frac{\epsilon_r}{\epsilon_b} - 1\right)$, where ϵ_r and ϵ_b are the relative permittivities of the target and the background medium, respectively. Eq. 1 is a linear inverse problem and can be solved by truncated singular value decomposition (TSVD), and final form of solution can be represented by [9]

$$\chi = \sum_{i=1}^{T} \frac{1}{\sigma_i} \langle \boldsymbol{f}, u_i \rangle v_i \qquad (2)$$

wherein $\{u_i, \sigma_i, v_i\}$ denotes the SVD of $\boldsymbol{G}$. Truncation number (T) is to be selected to filter out the insignificant singular values.

After obtaining the contrast function χ through the linear inverse problem described by Eq. 1, solved via truncated singular value decomposition (TSVD) as in Eq. 2, we

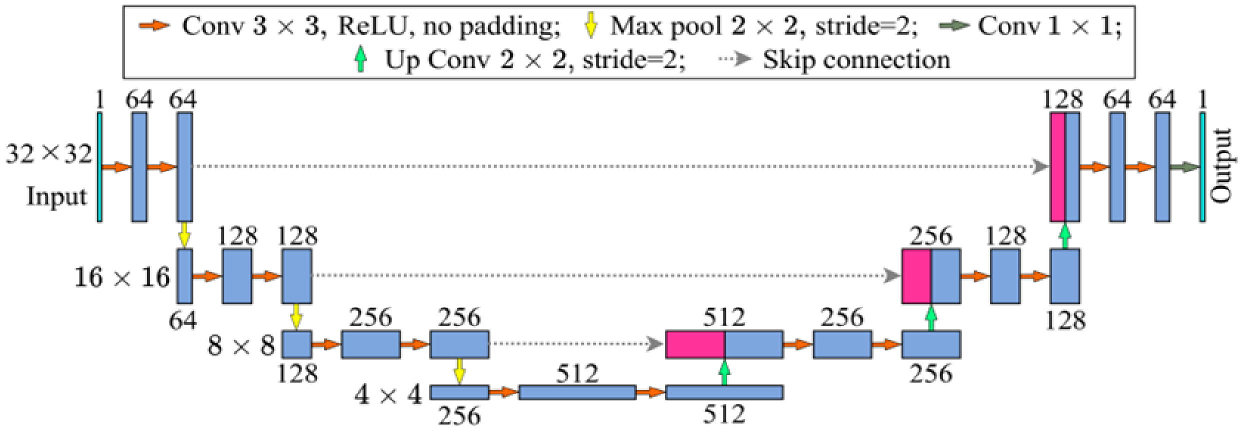

Figure 1. Architecture of U-Net

propose to enhance the accuracy and efficiency of tomographic reconstruction using a deep learning strategy. Specifically, the trained U-Net convolutional neural network will refine and map the estimated χ values to improve the reconstructed images as described in subsequent Sections.

3. Image Configurations

In bistatic multifrequency configuration, two antennas are used. One serving as the transmitting antenna (Tx) and the other as the receiving antenna (Rx) as shown in Fig. 2 . Both antennas are positioned near to the air-soil interface. The buried targets are illuminated with Tx at various frequencies, and the resulting scattered fields are measured at the receiver end (Rx). Subsequently, both antennas are moved together along the observation line (along the x-axis) with a fixed offset between them, and the measurement process is repeated for other required measurements. The advantages of this setup include its simplicity in hardware design (requiring only two antennas) and ease of inverse solution due to the relatively small number of measurements.

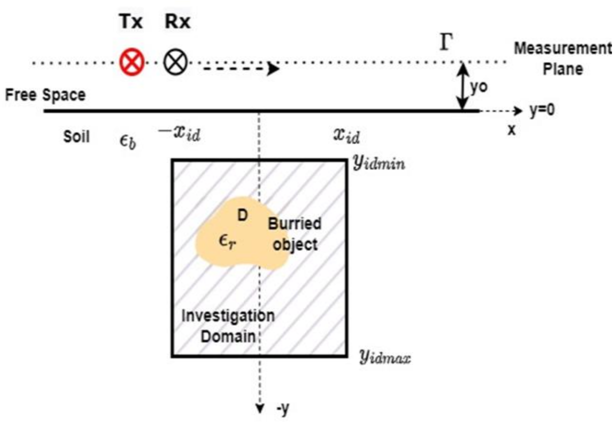

Figure 2. Measurement image configuration

If M number of measurements is performed for F number of frequencies then the total number of measurements is $(M \times F)$. The advantages of this setup are: It is a simple design from a hardware point of view (Only two antennas are required).

4. Architecture of The Network

The proposed CNN architecture is based on the U-Net, which is commonly used for image segmentation. Figure 1 depicts the proposed model, which uses a U-Net network with an encoder depth of 3. This model takes an 32×32 image from outputs of inverse algorithm and produces a super-resolution output of the same size. A set of convolutional layers and rectified linear units (ReLU) form the contracting path, which is followed by a max-pooling task. The objective of this path is to capture the input image's context. The expansive path is identical to the contracting path, except the contracting path's max-pooling is substituted by an up convolution. There are three concatenations in the expanding path with the corresponding feature maps from the contracting path. The expanding and contracting paths are then connected using the bridge, which consists of two convolutional layers and a dropout layer. In the expanded path, the blocks with two colors represent the concatenation of corresponding blocks. The use of skip connections allows for the recovery of fine-grained features, and enhance the optimization process by preventing the gradients from vanishing. In addition, the Softmax layer is removed, and a regression layer replaces the segmentation layer. More details about the architecture can be found in [3]

5. Training of The Network

The output from the Born approximation is used to train the CNN, as shown in figure 3. The training data contains 6561 reference profiles containing different circular objects. The mean square error is used as a loss function to train the network. This loss function is optimized using the Adaptive Moment Estimation (Adam) optimizer, with a learning rate of 0.0003. This optimizer is better than other optimizers at navigating through the loss surface. The model is trained for 50 epochs (150 iterations per epoch), with a batch size of 32. In addition, 0.5 dropout regularization is used to prevent over-fitting [6].

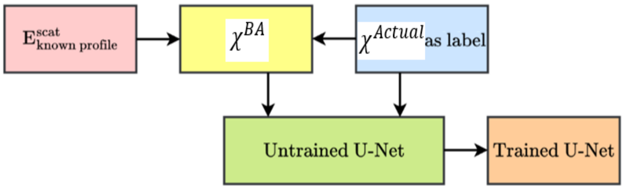

Figure 3. Training U-Net using Born approximated estimate (τ^{BA})

6. Numerical Results

Here, the dimension of investigation domain is $0.6m \times 0.6m$, with the center point of $(0m, -.32m)$. This region is divided into 1024 (32×32) square cells of length 0.01875m. The background is considered dry sand with a permittivity of $\epsilon_b = 3.2$. The transmitting and receiving antennas are located 0.05m above the ground surface. To quantify the efficiency of the stated algorithms, Relative Error (RE) is calculated, which is defined as

$$RE = \frac{\|\chi_r - \hat{\chi}_r\|}{\|\chi_r\|} \quad (3)$$

where χ_r and $\hat{\chi}_r$ represent the actual and the estimated contrast function, respectively. Two examples are considered. First example consists of square cylinder of length 0.1m and permittivity 6.7 (Fig. 4a(i)), second example consist of two identical cylinders of radius 0.04 m and permittivity 6.7 (Fig. 4a(ii)). A convolutional neural network based on U-Net is designed and trained using 6561 profiles. The reference profiles are made up of one or two circular cylinders with a radius of 0.06m that are positioned in every available region inside the investigation domain. The tomographic reconstruction result using BA multi frequency is shown in Fig. 4b(i). We considered 9 frequencies in the range of 200 MHz to 1800 MHz, with a step frequency of 200 MHz.). It can be observed that it can successfully reconstructs the object's location but the shape is deteriorated to some extent. Additionally, the relative error for this case is (0.7890). Deep-learning assisted BA is shown in Fig. 4c(i). The results show that this approach reconstructs the target quite accurately. Additionally, the relative error for this case is quite low (0.5589). Similar observations are found for the two cylinder case which are shown in the same figure. In the case of without DL, the error on reconstruction is 0.7654. Using DL, It has been observed that the reconstruction quality is very good in terms of imaging resolution and noise. Here, the output is free of any speckle artifacts. Additionally, the error on reconstruction is 0.3009.

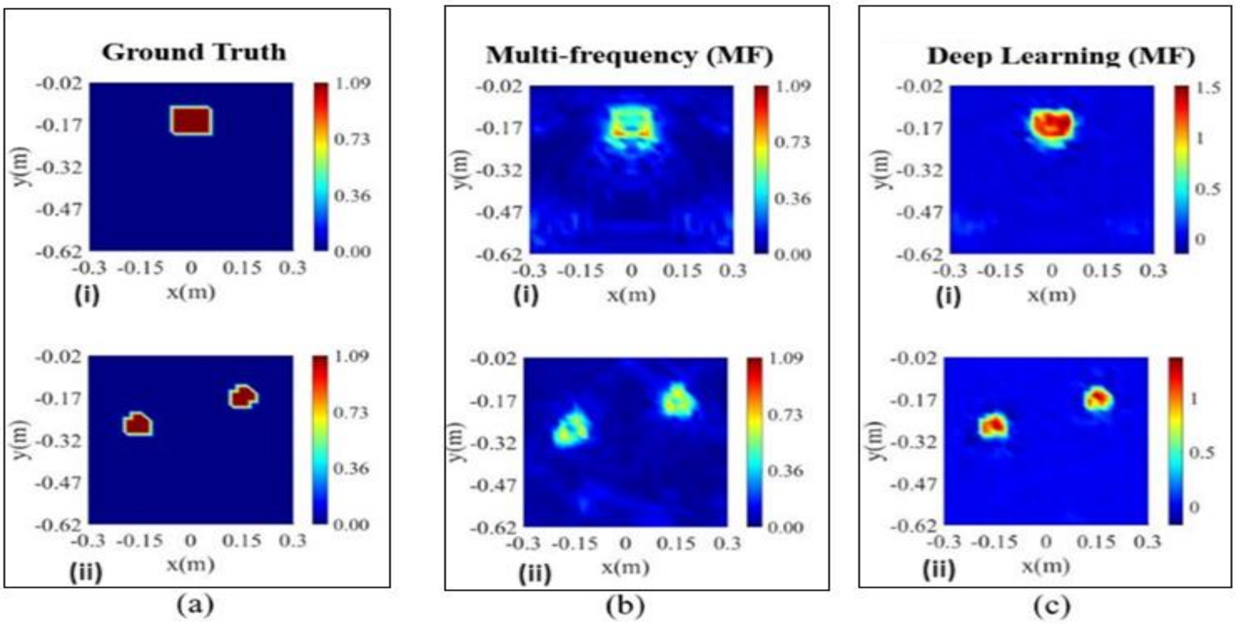

Figure 4. Tomographic reconstruction of square dielectric cylinder: (a) Reference profile. (b) Single-view case. (c) Bistatic case. (d) Multistatic case

7. Conclusions

This paper has explored the integration of deep learning techniques to enhance tomographic reconstruction using ground-penetrating radar (GPR). The U-Net convolutional neural network effectively refines the contrast function obtained via truncated singular value decomposition (TSVD), thereby improving the resolution and accuracy of reconstructed images. Numerical simulations demonstrate significant enhancements in detection accuracy, underscoring the potential of deep learning in advancing GPR tomography, especially in complex and noisy environments.

Future directions include optimizing deep learning architectures for real-time processing and extending the methodology to three-dimensional scenarios

8. Acknowledgements

The research work carried out in this paper is supported by the Core Research Grant, SERB, India, File no. CRG/2020/004127.

9. References

1. Harry M. Jol, Ground Penetrating Radar: Theory and Applications. Amsterdam, The Netherlands: Elsevier, 2009.

2. M. Ambrosanio, M. T. Bevacqua, T. Isernia and V. Pascazio, "he Tomographic Approach to Ground-Penetrating Radar for Underground Exploration and Monitoring: A More User-Friendly and Unconventional Method for Subsurface Investigation," *IEEE Signal Processing Magazine* , **36**, 4, July 2019, pp. 62-73. doi**:** 10.1109/MSP.2019.2909433

3. K. Xu, L. Wu, X. Ye and X. Chen, "Deep Learning-Based Inversion Methods for Solving Inverse Scattering Problems With Phaseless Data," *IEEE Transactions on Antennas and Propagation*, **68**, 11, Nov 2020, pp. 7457-7470. doi**:** 10.1109/TAP.2020.2998171

4. Yash Sanghvi, Yaswanth Kalepu, and Uday K Khankhoje, "Embedding Deep Learning in Inverse Scattering Problems," *IEEE Transactions on Computational Imaging* , **6**, 1, 2020, pp. 46–56. doi:10.1109/TCI.2019.2915580

5. J. Munk, "An equivalent source inversion method for imaging complex structures," Ph.D dissertation, Ohio State University, USA, 1999.

6. M. Li et al., "Machine Learning in Electromagnetics With Applications to Biomedical Imaging: A Review," in *IEEE Antennas and Propagation Magazine*, **63**, 3, June 2021, pp. 39-51. doi**:** 10.1109/MAP.2020.3043469

7. R. Persico, R. Bernini, and F. Soldovieri, "The role of the measurement configuration in inverse scattering from buried objects under the Born approximation," *IEEE Trans. Antennas Propagat.,* **53**, 6, 2005, pp. 1875–1887. doi**:** 10.1109/TAP.2005.848468

8. A. Giannopoulos, "Modelling ground penetrating radar by GprMax," *Construction Building Mater*., **19,** 10, 2005, pp. 755–762.

9. D. Comite, A. Galli, I. Catapano, and F. Soldovieri, "The role of the antenna radiation pattern in the performance of a microwave tomographic approach for GPR imaging," *IEEE J. Sel. Topics Appl. Earth Observ. Remote Sens.*, **10**, 10, 2017, pp. 4337–4347. doi**:** 10.1109/JSTARS.2016.2636833

10. M. Ambrosanio, M. T. Bevacqua, T. Isernia and V. Pascazio, "Performance Analysis of Tomographic Methods Against Experimental Contactless Multistatic Ground Penetrating Radar," *IEEE Journal of Selected Topics in Applied Earth Observations and Remote Sensing*, **14**, 2021, pp. 1171-1183.
doi: 10.1109/JSTARS.2020.3034996